

05,11

Magnetocaloric effect in amorphous-crystalline microcircuits PrDyFeCoB© E.V. Dvoreckaia¹, V.L. Sidorov¹, O.V. Koplak¹, D.V. Korolev², V.P. Piskorsky²,
R.A. Valeev², R.B. Morgunov^{1,2,3,¶}¹ Institute of Problems of Chemical Physics, Russian Academy of Sciences,
Chernogolovka, Moscow oblast, Russia² All-Russia Institute of Aviation Materials (VIAM),
Moscow, Russia³ Tambov State Technical University,
Tambov, Russia

¶ E-mail: morgunov2005@yandex.ru

Received May 1, 2022

Revised May 1, 2022

Accepted May 2, 2022

In amorphous-crystalline PrDyFeCoB microconductors obtained by ultrafast melt cooling, a negative magnetocaloric effect was detected at 200–250 K (with heat release when the magnetic field is turned on), as well as a positive magnetocaloric effect in the temperature range of 300–340 K (with heat absorption when the magnetic field is turned on). It is established that there are no phase transitions of the first kind in the studied temperature range, which indicates that both of the detected effects are associated with a change in the magnetic part of the entropy. The transition at 200–250 K is due to the presence of metamagnetic states induced by a magnetic field in the spin-glass state of the amorphous part of the PrDyFeCoB alloy, and with their transition to the ferrimagnetic state. The transition at 300–340 K is spin-reorientation, and it occurs in crystalline inclusions identified in the amorphous matrix. Keywords: spin-reorientation transition, spin glass, magnetocaloric effect, entropy.

Keywords: spin-reorientation transition, spin glass, magnetocaloric effect, entropy.

DOI: 10.21883/PSS.2022.08.54615.373

1. Introduction

The magnetocaloric effect (MCE) offers a simple way to achieve environmentally friendly energy-saving cooling in the long run. The MCE is that when a sample is placed in a magnetic field, a phase transition can occur in it that changes the ordering of the magnetic moments and the corresponding part of the magnetic entropy [1,2]. Such a conversion during an abrupt adiabatic change in the magnetic field can lead to a change in the sample temperature and can be effective provided that the magnetic part of the entropy changes sufficiently much. In isothermal slow change of magnetic field, the temperature of the sample remains constant, but the magnetic part of entropy changes ΔS_M . If phase transitions of the first kind are absent, the MCE is reduced to a change in the magnetic part of entropy caused by the reorientation of magnetic moments. The strongest entropy changes obviously occur at transitions involving a completely disordered state, such as the paramagnetic state or the spin glass state. Spin-glass states and transitions in them to a magnetically ordered state under the action of a magnetic field are known in the literature. For example, in PrDyFeCoB amorphous-crystalline microwires, there is a spin-flip transition between the ferrimagnetic state and the spin glass state [3,4].

On the one hand, this suggests that such a transition may involve a significant change in the magnetic part of entropy, because the disorder–order transition in the spin subsystem

gives the largest possible value of ΔS_M . On the other hand, the presence of rare-earth ions Dy³⁺ and Pr³⁺ with high spin values also works in favor of strengthening the MCE. If an alloy transitions from a completely disordered spin-glass state to a completely ordered magnetic state, the expected maximum possible change in magnetic entropy during this transition ΔS_M depends on the multiplet $2J + 1$, where J — the total angular momentum and is defined by the formula [1]:

$$\Delta S_M = R \ln(2J + 1), \quad (1)$$

where R is the universal gas constant.

In the trivalent rare-earth ions of the second half of the lanthanoid group (heavy elements Dy³⁺ and Pr³⁺), the main multiplet is $J = |L + S|$, and it provides high values J in Pr³⁺ ions with shell $4f^2$ ($S = 1$, $L = 5$, $J = 4$; term (³H₄)) and in Dy³⁺ ions with shell $4f^9$ ($S = 5/2$, $L = 5$, $J = 15/2$; term (⁶H_{15/2})). In rare-earth alloys containing Gd³⁺ ions, record values of MCE [5,6] were found. The advantage of using the PrDyFeCoB alloy could be the strong dependence of the spin-flip transition temperature on the applied magnetic field [3,4] (Fig. 1).

In addition to these simple technical considerations in favor of the PrDyFeCoB alloy, there are several reasons to look for new fundamental effects in it related to magnetocaloric properties.

First, almost all of the materials studied exhibit positive MCE near room temperature, associated with the Curie

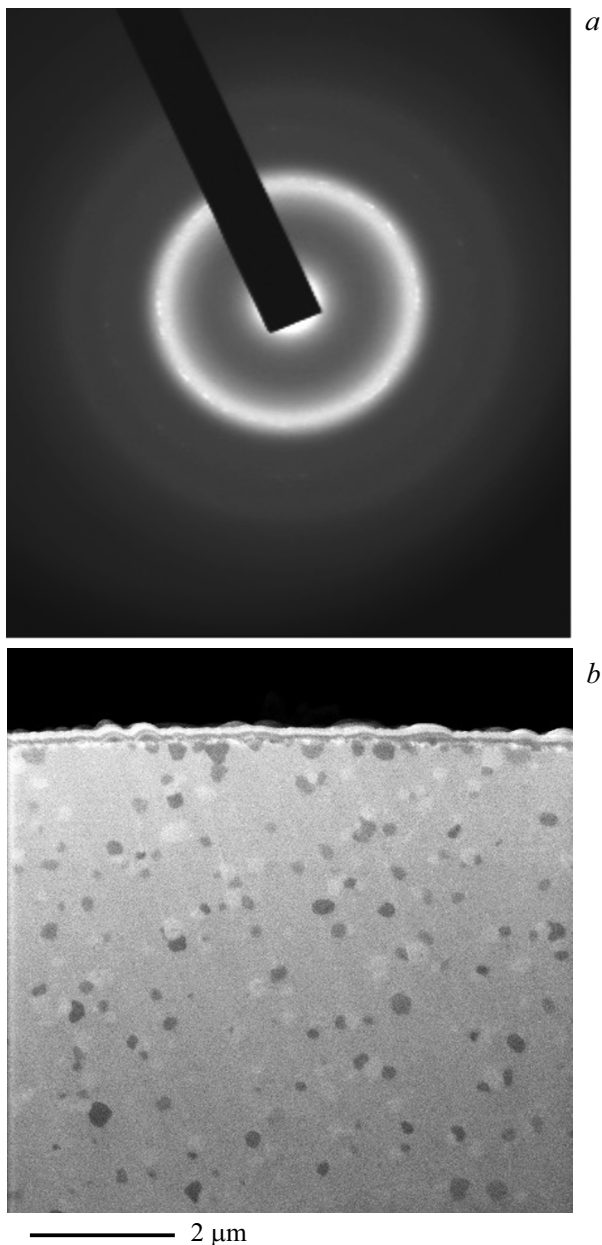


Figure 1. *a* — electron diffraction of microwires by HR-TEM data; *b* — micro-inclusions in the amorphous matrix revealed by the microwire end study in SEM.

point transition. As far as the authors know, only the FeRh [7] and $\text{Ni}_{2+x}\text{Mn}_{1-x}\text{Sn}$ [8] meta-magnetics showed a significant negative magnetocaloric effect, i.e. reduction of the material temperature when the magnetic field is activated. Since, according to the theory of spin glasses [9,10], full spin disordering in them takes place only in the absence of a magnetic field, and as the field increases, fan, sphero-magnetic, and meta-magnetic structures arise, which transition to a ferro or ferrimagnetic state in strong fields, we can expect the PrDyFeCoB alloy to exhibit negative MCE, going from spin-glass to ferromagnetic state as the field increases.

Second, the principal feature of the PrDyFeCoB alloy is the very high single-ion anisotropy of the Dy^{3+} and Pr^{3+} ions, which exceeds the exchange interaction energy, and in the spin glass state leads to the fact that chaotic variations in the directions of local anisotropy axes give the alloy properties of spin glass. This significantly distinguishes the type of spin glass PrDyFeCoB from the traditionally considered alloys, which require an amorphous state of atomic structure providing variations in the interatomic distances and exchange interaction between spins. In alloy PrDyFeCoB, the atomic structure of the material does not necessarily have to correspond to an amorphous state for spin-glass states to occur. This unique type of spin glass was discovered in the works of Almeida [11] and Taulez [12] and was confirmed in our works when studying PrDyFeCoB microwires. The non cramer ions Dy^{3+} and Pr^{3+} have significant anisotropy, in directions perpendicular to the light axis of single-ion anisotropy. Such ions are called ising ions.

Third, in the crystalline state, the tetragonal phase $(\text{PrDy})_2(\text{FeCo})_{14}\text{B}$ has a very high coercivity 2–2.5 T at room temperature [13–15], which also results from the high single-ion anisotropy of Dy^{3+} and Pr^{3+} . Since the fundamental cause of the single-ion magnetic anisotropy is the high value of the spin-orbit interaction in Dy^{3+} and Pr^{3+} ions, one would expect the orbital moment to make an contribution to the magnetic part of the anisotropy and its change in magnetic field in crystallites, which are usually in the amorphous phase, when studying MCE.

Finally, an additional degree of freedom in the regulation of the MCE in the PrDyFeCoB alloy is associated with the possibility of substitution of Dy^{3+} and Pr^{3+} ions for other rare-earth ions and the presence of two sublattices of PrDy and FeCo with negative antiferromagnetic interaction between them. All this can lead to unusual manifestations of MCE in the PrDyFeCoB alloy.

The aim of the work was to create experimental conditions for isothermal measurement of the magnetic part of the entropy ΔS_M and its changes in the magnetic field 0–5 kOe in the temperature range of spin glass-ferrimagnetic transition 190–340 K in the amorphous spin-glass state of PrDyFeCoB alloy, which occurs in microwires obtained by superfast cooling of the melt. In addition, one of the goals was to determine the contribution of crystalline ferromagnetic inclusions in MCE.

2. Experimental methods and samples

The microwires were obtained by hanging drop melt extraction (HDME) of PrDyFeCoB. The melt was created by heating the face of the sintered magnet with an electron beam. A drop of melt was captured by a rapidly rotating water-cooled brass cylinder, which pulled it into a long filament, which was cooled by thermal contact with the cylinder at a rate of about $\sim 10^6$ K/s. At high cylinder rotation speeds ~ 40 –50 m/s, microwires with an amorphous phase fraction of up to 86 at.% are

formed. Crystalline ferrimagnetic phases 1–4–1, 2–1 are also present in microwires. The resulting microwires had a diameter of 60–100 μm and a length of 5–10 mm. The magnetic moment of the microwires was measured with an MPMS XL Quantum Design magnetometer at temperatures near the previously detected phase transition of the second kind 60–350 K and in magnetic fields $H = 0\text{--}5\text{ kOe}$. The external magnetic field was directed along the microwire, because this orientation produces the largest magnetic moment jump during the spin-flip transition [3,4]. The curves $M(H)$ were obtained with a slow isothermal magnetic field rise, so that each was measured at a fixed cryostat temperature. A series of such curves was obtained at different temperatures in increments of 5 K to further calculate the magnetic part of the entropy. Differential scanning calorimetry was used to confirm the existence of the detected MCE.

In addition, the temperature dependences of the longitudinal magnetic moment $M(T)$ were obtained in two modes: 1) FC (field cooling), which corresponds to the measurement of the magnetic moment when the sample is heated in a weak magnetic field of 100 Oe after its cooling in a strong field of 5 kOe, 2) ZFC (zero field cooling), which corresponds to the measurement of the magnetic moment when the sample is heated in a weak magnetic field of 100 Oe after its cooling in zero field. The residual magnetization M_{rem} was measured in zero field.

Scanning electron microscope (SEM) images of microwires were obtained using the TescanClara super-resolution complex at 15 kV accelerating voltage on a cross section prepared by ion etching and polishing in the TechnoorgLinda SEMPrep2 complex. The microwire structure was analyzed by electron diffraction in a high resolution transmission electron microscope HRTEM JEOL.

Differential scanning calorimetry in a magnetic field was performed using the LKH-500 complex. In each experiment, the cell with and without sample filled with polyethylsiloxane oil (PES-4) had its own initial temperature (the base dotted line in the graphs), relative to which the temperature jump of the microwire was estimated.

3. Experimental results and discussion

3.1. Chemical and phase composition of microwires

According to the HRTEM electron transmission microscopy data, the microwires contained amorphous phase, the fraction of which varied in the range of 50–80 at.% from sample to sample (Fig. 1, *a*), as well as micro-inclusions (Fig. 1, *b*). Since the electronogram shows solid rings, indicating the presence of significant structural disorder, the samples are amorphous material with nanocrystalline inclusions. In Fig. 1, *b*, in addition to solid rings, the diffraction pattern contains point reflexes, which are caused by the presence of inclusions.

Fig. 2 shows the SEM image of the microwire end *I* (Fig. 2, *a*) and Fig. 2, *b–e* results of energy dispersive chemical analysis (EDX) as chemical element distributions of Fe, Co, Pr, Dy obtained on the microwire end *I* (Fig. 2, *b–e*).

An increase in brightness corresponds to an increase in the concentration of each element. In Fig. 2, *b* you can clearly see light areas of size 0.5–1 μm , which correspond to local iron enrichment, although no change in the concentration of cobalt in these areas is observed (Fig. 2, *c*). In Fig. 2, *d* you can see that in the same areas there is a dimming, which corresponds to a decrease in the concentration of Pr. In this case, there is an enrichment of these areas Dy (Fig. 2, *e*). Since the inclusions have an increased concentration of Dy and Fe, we most likely observe inclusions of the DyFe or DyFeB type (B not determined by the EDX method).

Thus, the microwires were an amorphous matrix of PrDyFeCoB containing crystalline inclusions of DyFe or DyFeB.

3.2. Almeida–Taulez spin-flip transition in the amorphous part of the microwire

In our work [3,4] we reported a spin-flip transition in the amorphous part of PrDyFeCoB microwires (Fig. 3), and it was found that the magnetization approximation to saturation and the magnetic relaxation dynamics satisfy the predictions of the Ising [16] spin glass theory.

Figure 3, *a* shows the temperature dependences of the microwire magnetic moment, obtained at different values of the external field 0–10 kOe, directed along the microwire axis. The microwires were first cooled in a zero field to a temperature of 60 K, and then the magnetic field was switched on and the temperature dependence was measured while the sample was being heated. It can be seen that the temperature dependences of $M(1/T)$ in the high-temperature area deviate significantly from the Curie–Weiss dependence and show a jump change in the microwire magnetic moment at different critical temperatures T_c (shown by arrows for 0 and 10 kOe). The critical temperature T_c decreases with increasing magnetic field, as described for the spin-flip transition in spin-glass rare-earth alloys [16–18]. The regularities of this spin-flip transition were first described in de Almeida and Thouless (de Almeida–Thouless) [18]. The authors applied Sherrington–Kirpatrick [17] flow theory to describe the magnetization of local areas of the DyFeB Ising spin glass, predicting the critical field at which magnetization islands would merge (the percolation limit) and a ferromagnetic state would emerge from the original spin-glass state. From the theory follows a formula that relates the critical magnetic field H of the magnetic phase transition between a Heisenberg spin glass and a ferromagnet to the temperature T :

$$H^2 = A(1 - T/T_c)^3. \quad (2)$$

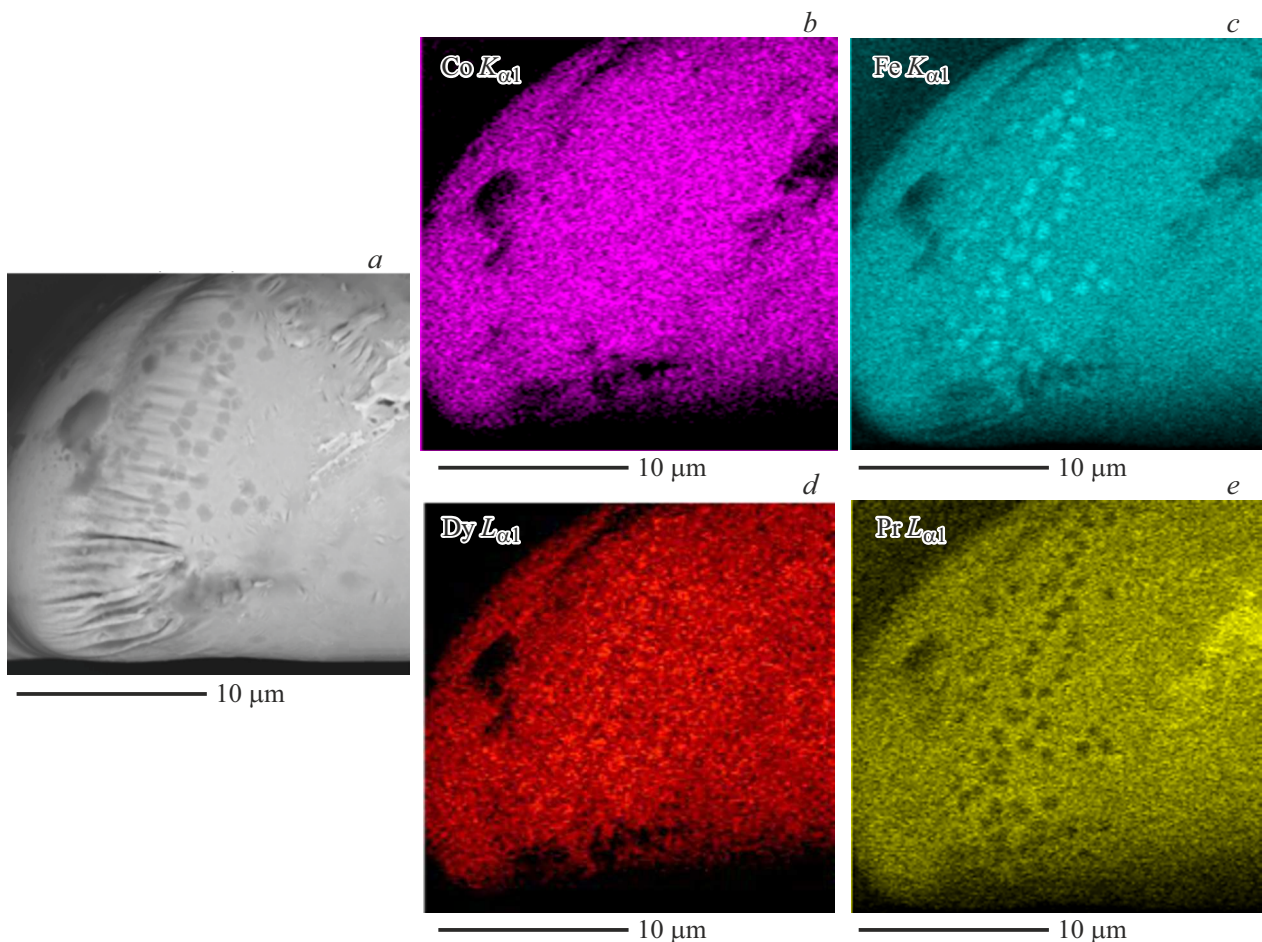


Figure 2. *a* — SEM image of the microwire end *1*, *b–e* — distributions of chemical elements on the microwire end *1* determined by EDX method. An increase in brightness corresponds to an increase in the concentration of the element.

This function separates the areas of existence of spin-glass (SG) and ferrimagnetic (FM) states in the coordinates $H-T$. Figure 3, *b* (curve 1) shows the dependence of the critical field H^2 on the normalized temperature $(1-T/T_c)^3$ for DyPrFeCoB microwires, which is close to linear, as it should be if ratio (2) is met. Figure 3, *b* (curve 2) shows the work [17] data in spin glass Dy₁₆Cu₁₂Fe₇₂ for comparison. The approximation results are shown by solid lines. Thus, the spin-flip transition in the amorphous part of microwires is well described by spin glass theory. Such a transition of the second kind can be the basis for the magnetocaloric effect.

3.3. Blocking temperature in micro-conductors with nanocrystalline inclusions

The presence of micro-inclusions in microwires leads to other properties that are more characteristic of ferromagnetic nanoparticles than of the amorphous matrix. In particular, there is a difference in the temperature dependences recorded in the measuring field 50 Oe after cooling the sample in the strong field 5 kOe (1) and without field (2) (Fig. 4, *a*). These dependences are usually

called FieldCooling, FC (1) and ZeroFieldCooling, ZFC (2). They intersect at a temperature $T_b = 300$ K, which can be interpreted as the blocking temperature of the magnetization of crystalline ferromagnetic nanowires in the microwire. If you increase the measuring field to 500 Oe, the blocking temperature decreases to $T_b = 195$ K (Fig. 4, *b*).

The decrease in the blocking temperature with increasing measuring magnetic field in such experiments is explained by the slope of the potential relief formed by the magnetic anisotropy profile summarized with the Zeeman energy of the nanoparticle. The effective height of the barrier separating the opposite directions of nanoparticle magnetization decreases as the Zeeman energy [19] increases. The blocking temperature depends on the field according to the formula

$$T_b(H) = KV(1 - H/H_b)^2/k_B \ln(\tau_m/\tau_0), \quad (3)$$

where τ_m — the measurement time, τ_0 — the time between attempts to overcome the barrier, K — the anisotropy constant, V — the nanoparticle volume, H_b — the critical field of overcoming the potential barrier. The latter value can

be determined by applying ratio (2) at 50 Oe and 500 Oe:

$$T_{b1}/T_{b2} = (1 - H_1/H_b)^2 / (1 - H_2/H_b)^2. \quad (4)$$

From expression (4) with values $T_{b1} = 300$ K, $T_{b2} = 195$ K, $H_1 = 50$ Oe, $H_2 = 500$ Oe follows $H_b = 900$ Oe. The low value of the critical field of overcoming the barrier is advantageous for the manifestation of MCE in low fields.

Thus, in addition to the amorphous matrix, crystalline nano-inclusions can also contribute to the magnetocaloric effect, since their blocking temperatures are in the 200–300 K area at the magnitude of the fields used in our experiments.

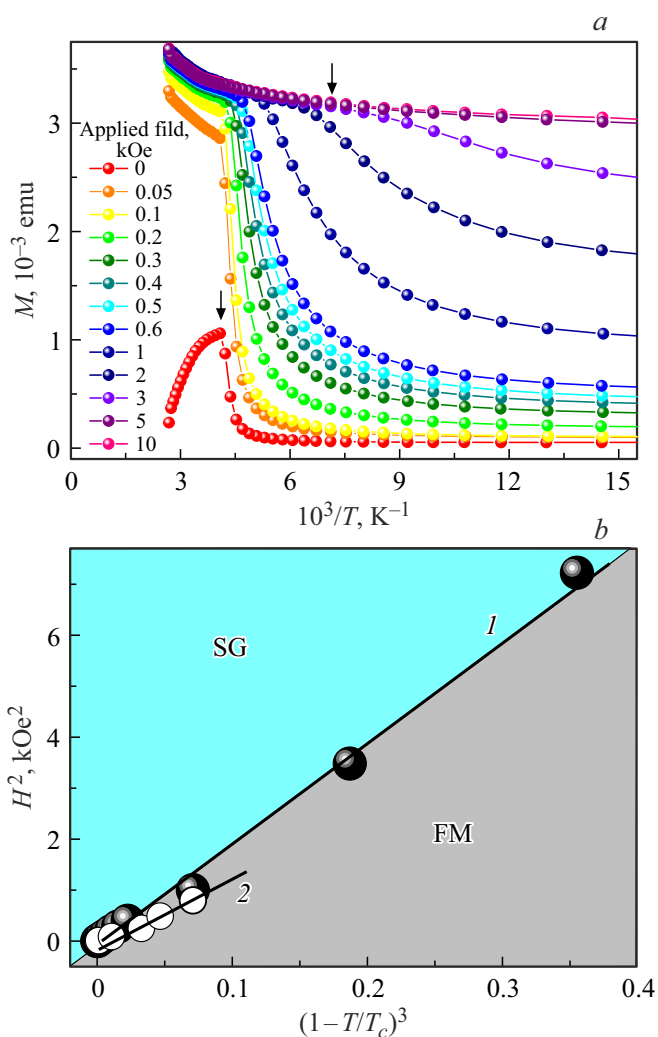


Figure 3. *a* — dependences of the microwire magnetic moment on the inverse temperature in the magnetic field directed along the microwire axis. The vertical arrows show the critical temperatures T_c for comparison. *b* — dependences of the normalized transition temperature $(1 - T/T_c)^3$ on the square of the magnetic field H^2 applied along the microwire axis when heating the sample from 2 K in the field directed along the microwire axis in DyPrFeCoB microwires (1) in this work and (2) in [17] in the spin glass Dy₁₆Cu₁₂Fe₇₂. The solid line shows the theoretical dependences predicted by the Almeida–Taulez theory [18].

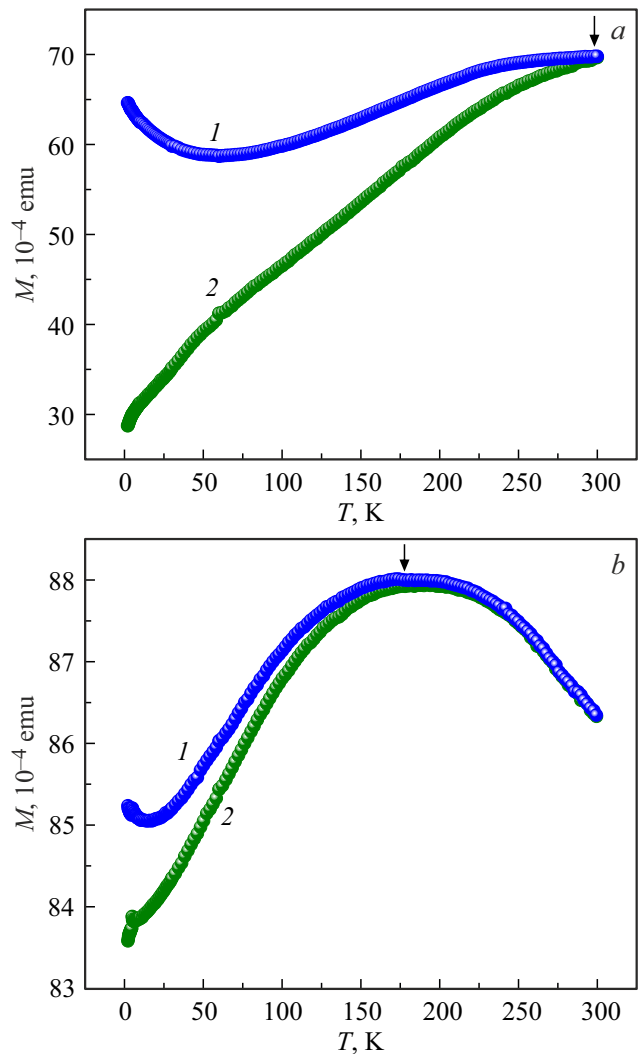


Figure 4. Temperature dependences of microwire magnetic moment measured in 50 Oe (*a*) and 500 Oe (*b*) magnetic fields after cooling (1) in 5 kOe magnetic field (FC) and (2) without sub-magnetizing field (ZFC). The arrows show the blocking temperatures in the 50 Oe (*a*) and 500 Oe (*b*) fields.

3.4. Isothermal measurement of the magnetic part of entropy

To calculate the magnetic part of the entropy, we obtained the field dependences of magnetization in isothermal mode, when the field increased slowly enough (33 Oe/min) so that the sample was in thermal equilibrium with the magnetometer chamber and did not change its temperature. From the extensive series of isothermal curves we have recorded, several examples at various temperatures are shown in Fig. 5, *a*.

The basis for calculating changes in total entropy is Maxwell’s equation, which relates changes in entropy and magnetic moment [16]:

$$\left(\frac{\partial S}{\partial H}\right)_T = \left(\frac{\partial M}{\partial T}\right)_H. \quad (5)$$

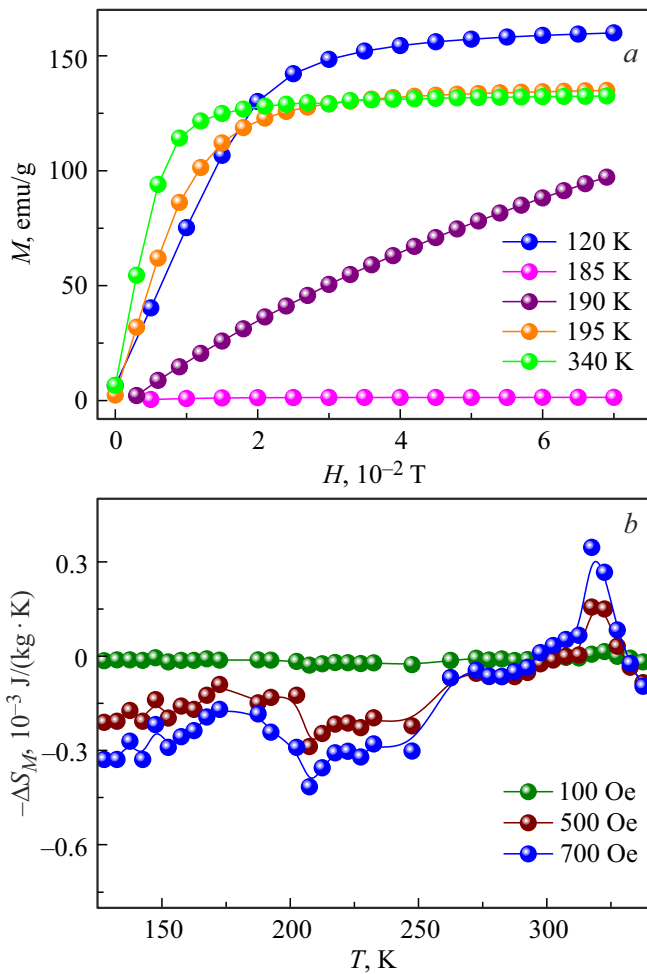


Figure 5. *a* — isothermal dependence of the magnetization of the microwire in the temperature range 120–300 K. *b* — temperature dependence of the change in the magnetic part of the entropy.

Maxwell's equation (5) refers to the total entropy S , which includes the phonon, electron, and magnetic parts. For the second kind transitions considered in our work, the Maxwell equation can be transformed into the Clausius–Clapeyron equation:

$$\Delta S/\Delta M = -dH/dT. \quad (6)$$

Equation (6) is strictly valid for calculating the change in the magnetic part of the entropy ΔS_M alone if there is no temperature hysteresis, which we found in separate experiments. A series of isothermal magnetization curves were used to calculate the magnetic part of the entropy S_M and its change $\Delta S_M(H, T)$ caused by spin-flip transitions (Fig. 5, *b*). The expression for calculating the magnetic part of the entropy can be obtained from (6) [16]:

$$\Delta S_M(T, H) = \int_0^H \left(\frac{\partial M(T, H)}{\partial T} \right)_H dH. \quad (7)$$

Since in real experiments the temperature and magnetic field change discretely, expression (7) is usually rewritten as a discrete formula

$$\Delta S_M(T, H_0) = \sum_i \frac{M_{i+1}(T_{i+1}, H) - M_i(T_i, H)}{T_{i+1} - T_i}. \quad (8)$$

$M_i(T_i, H)$ — magnetic moment at temperature T_i , $M_{i+1}(T_{i+1}, H)$ — magnetic moment at temperature T_{i+1} . The dependence $-\Delta S_M(H, T)$ obtained this way is shown in Figure. 5, *b*. It can be seen that in the area of 200–250 K there is a negative MCE, while in the area of 300–340 K there is a positive MCE.

The obtained data allow to calculate the main magnetocaloric parameters of microwires for positive MCE at 700 Oe: the maximum change of magnetic part of entropy $-\Delta S_m \sim 0.35$ mJ/kg·K, and the relative cooling power $RCP = 0.007$ J/g. The latter characteristic was calculated according to the formula [16]:

$$RCP = -\Delta S_m \Delta T_{1/2}, \quad (9)$$

where $\Delta T_{1/2} = 10$ K is the half-width of the maximum on the dependence $-\Delta S_M(T)$ (Fig. 5). For the negative MCE corresponding to the minimum in Fig. 5, *b*, the following parameters were obtained: $-\Delta S_m \sim -0.4$ mJ/kg·K, $RCP \sim 0.04$ J/g.

Although the values obtained are not record values and cannot compete with the maximum values obtained in the literature for Gd alloys, they are quite acceptable for technical applications.

3.5. Isothermal measurement of the magnetic part of entropy

The above results of calculating the magnetic part of entropy are, to a certain extent, indirect, although widely used method of research MCE. This section discusses the MCE detected by differential scanning calorimetry (DSC). In the course of the experiment, the field strength increased sharply from zero to the selected maximum value, which led to changes in the temperature of the sample. Thus, we plotted the dependences of the sample temperature change on the maximum values of magnetic field strength $\Delta T(H)$ (Fig. 6). The reverse experiment was also conducted when the magnetic field was completely switched off from the maximum value. In this case, the change in sample temperature ΔT changed the sign.

During measurements near 300 K, a positive MCE was detected, which was expressed as an increase in the sample temperature with a sharp increase in the strength of the generated magnetic field (Fig. 6).

This can be judged by the excess of the slope of the linear dependence $\Delta T(H)$ for the cell with the sample over the slope of the reference dependence $\Delta T(H)$ recorded for the cell without the sample (dotted line) (Fig. 6, *a*). If the magnetic field was turned off, the opposite effect

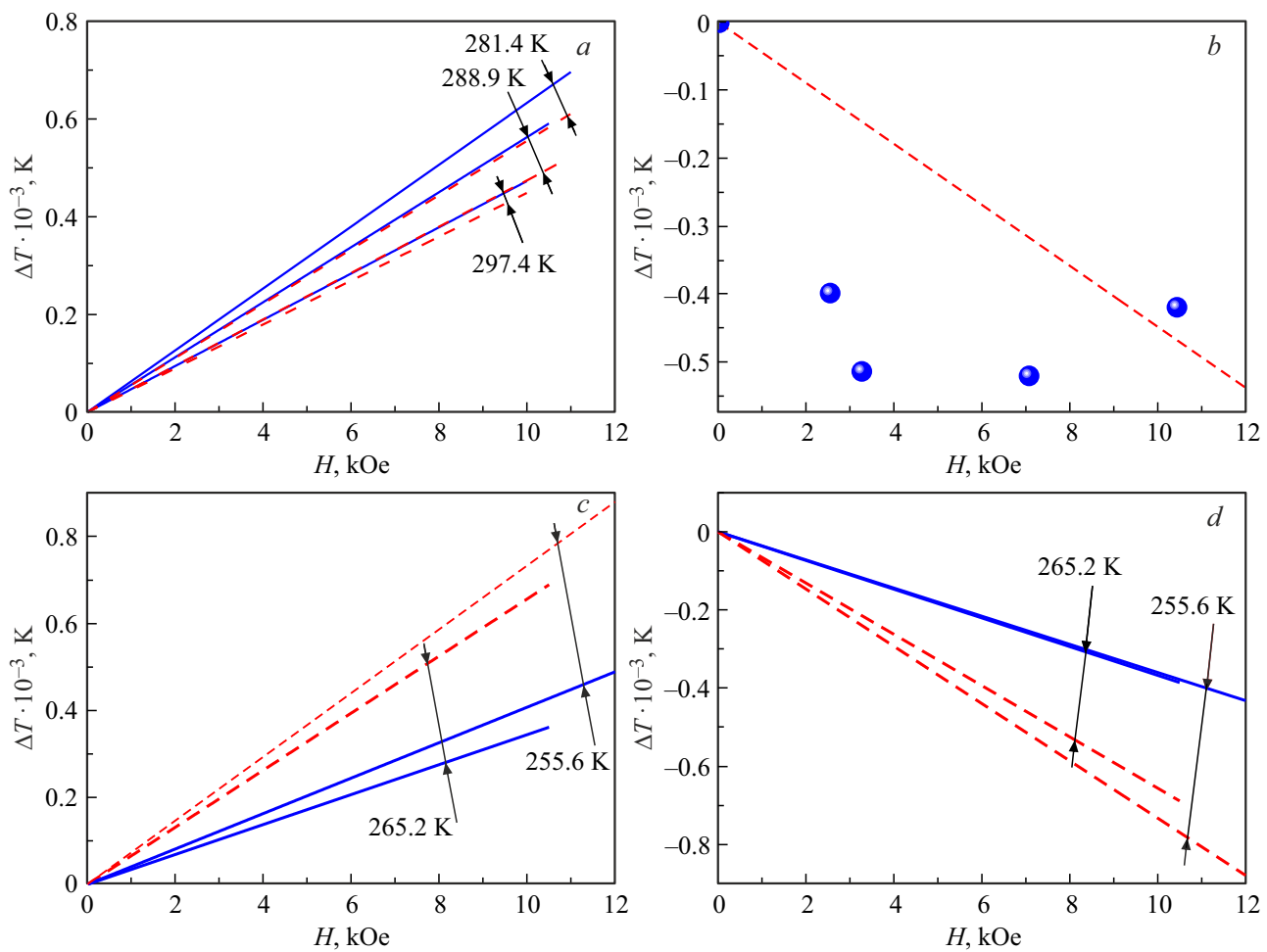


Figure 6. Dependences of temperature increase on the field for microwires in the PES-4 chamber (black) and for the PES-4 chamber without samples (red/dotted line): *a* — heating of the sample when introduced into the magnetic field, *b* — cooling of the sample when the field is turned off (for temperature 297.4 K), *c* — cooling of the sample when introduced into the magnetic field, *d* — heating of the sample when the field is turned off.

occurred — the temperature of the sample decreased. The maximum effect was reached at 297.4 K (Fig. 6, *b*).

Measurements in the 250 K area showed the presence of a negative MCE, which manifested itself in a decrease in the temperature of the sample with an increase in the magnetic field. The field dependences of the temperature increase $\Delta T(H)$ now have a reduced slope compared to the reference cell without sample (Fig. 6, *c*). If the magnetic field is switched off, the situation is the opposite — the sample is heated (Fig. 6, *d*).

4. Discussion

In the field of rare-earth alloys *Re-TM-B* (*Re* — rare-earth metals, *TM* — transition metals, *B* — boron) a considerable amount of research on the magnetocaloric effect has been done on bulk samples [13–25]. Studies of micro-magnets exhibiting MCE are not so widely presented in the literature. Let us briefly analyze the parameters

reached in the literature, comparing them with the MCE parameters in the present paper. The alloys $\text{Pr}_{1.3}\text{Nd}_{0.7}\text{Fe}_{17}$ and $\text{Pr}_{1.5}\text{Nd}_{0.5}\text{Fe}_{17}$ possess a rhombohedral crystal lattice of the $\text{Th}_2\text{Zn}_{17}$ [18] type, give maximum changes in the magnetic entropy component of 4.31 J/kg · K, an order of magnitude larger than in our experiments. The authors note that the relatively weak interaction of iron and rare-earth metal sublattices in R_2Fe_{17} alloys significantly reduces the entropy change near the Curie temperature. Due to the Curie temperature $T_c = 307$ K, close to room temperature, and the high value of $RCP = 487$ J/g, the $\text{Pr}_{1.3}\text{Nd}_{0.7}\text{Fe}_{17}$ alloy has the potential to provide efficient cooling at room temperatures. Note that the RCP value in $\text{Pr}_{1.3}\text{Nd}_{0.7}\text{Fe}_{17}$ is comparable in value to the data of our experiments, which is explained by the significant width of the entropy peak in the alloys we study. Magnetocaloric parameters of rare-earth alloys (Curie temperature T_c , maximum change in the magnetic component of entropy $-\Delta S_{\max}$, RCP) are collected in the Table according to data [13–25].

Magnetocaloric parameters of rare-earth alloys (Curie temperature T_c , maximum change in the magnetic component of entropy $-\Delta S_{\max}$, RCP) by data [13–25]

Compound	T_c , K	$-\Delta S_{\max}$, J/kg · K		RCP , J/kg		Reference
		20 kOe	50 kOe	20 kOe	50 kOe	
DyCo ₂ B ₂	10	5.4	12.1	88	282	[13]
DyCo ₃ B ₂	22	7.4	12.6	154	397	[13]
PrNdFe ₁₇	310	2.8	6	56	120	[14]
Pr _{1.3} Nd _{0.7} Fe ₁₇ (HDME)	307	2	4.3	110	487	[15]
Pr _{1.5} Nd _{0.5} Fe ₁₇ (HDME)	302	1.2	3.0	66	345	[15]
ErNi (HDME)	10	12.5	24	133	432	[22]
ErNi	10	15	29	300	510	[22]
Pr ₂ Fe ₁₇	292	–	6.4	–	160	[23]
Pr ₂ Fe ₁₇	285	2.8	5.5	70	138	[24]
Pr _{1.75} Dy _{0.25} Fe ₁₇	299	4.6	7.3	115	183	[24]
PrCo ₂	42	6.9	10.7	52	192	[25]
Pr _{0.8} Dy _{0.2} Co ₂	66	1.5	3.2	13	71	[25]
Pr _{0.6} Dy _{0.4} Co ₂	83	1.3	2.2	10	31	[25]
Pr _{0.4} Dy _{0.6} Co ₂	100	3.0	5.2	26	115	[25]
Pr _{0.2} Dy _{0.8} Co ₂	122	5.5	8.9	41	188	[25]
DyCo ₂	151	6.8	10.4	60	291	[25]

It follows from the data presented that the phase transition temperatures investigated in our and other works are close to room temperature. For example, the alloys (Pr_{2-x}Nd_x)Fe₁₇ are also characterized by phase transition temperatures close to the operating temperature of 300 K and have larger changes in the magnetic part of entropy and parameters RCP than in the present work. The use of rapid quenching, typical of the HDME method, to obtain the ErNi [22] alloy slightly reduces the resulting RCP values due to the formation of an amorphous phase. In the case of iron Pr_{2-x}Dy_xFe₁₇ [24] and cobalt (Pr_{1-x}Dy_x)Co₂ [25] alloys, replacement of praseodymium with dysprosium can extend the temperature range of the magnetic entropy burst, thereby increasing the parameter RCP . The increase of the magnetocaloric effect in DyPrFeCoB microwires can be further achieved by optimizing the chemical and phase composition.

5. Conclusions

1. In amorphic-crystalline microwires of PrDyCoFeB a negative magnetocaloric effect has been detected, which consists in reducing the magnetic part of the entropy during adiabatic magnetic field growth in the temperature area 200–240 K. In this area, a spin-flip Almeida-Taulez transition is observed between the spin glass state and the ferrimagnetic state of the amorphous part of the microwire.

2. At higher temperatures 300–340 K a positive magnetocaloric effect was found, which consists in an increase of the magnetic part of entropy during isothermal magnetic field accretion. This effect is related to the spin-flip transition in crystalline inclusions. The presence of DyFeB inclusions

of size 0.5–1 μm and Pr inclusions of size 5 μm in the amorphous matrix were identified by electron microscopy.

3. The closeness of the detected magnetocaloric effects to room temperature and the high single-ion anisotropy of rare-earth ions in the alloy allow us to hope for possible practical applications of the detected effects. The micron size of the microwires is an important condition for improving heat transfer when using an array of microwires as the working body of the refrigerator.

Financial support of work

The work has been performed within the thematic chart of the Institute of Problems of Chemical Physics AAAA-A19-119092390079-8.

Conflict of interest

The authors declare that they have no conflict of interest.

References

- [1] A.K. Zvezdin, V.M. Matveev, A.A. Mukhin, A.I. Popov. Redkozemelnyie iony v magnitouporyadochennykh kristallakh. Nauka, M. (1985). 295 p. (in Russian).
- [2] Ch. Hai-Ying, Z. Yan, Y. Yun-Bo, Ch. Xue-Gang, L. Shun-Quan, W. Chang-Sheng, Y. Ying-Chang, Y. Jin-Bo. Chin. Phys. Lett. **28**, 7, 077501 (2011). <https://doi.org/10.1088/0256-307X/28/7/077501>
- [3] R.B. Morgunov, O.V. Koplak, V.P. Piskorskii, D.V. Korolev, R.A. Valeev, A.D. Talantsev. J. Magn. Magn. Mater. **497**, 166004 (2020). <https://doi.org/10.1016/j.jmmm.2019.166004>

- [4] O.V. Koplak, E.V. Dvoret'skaya, D.V. Korolev, R.A. Valeev, V.P. Piskorskiy, A.S. Denisova, R.B. Morgunov. *FTT* **62**, 1187, 2020(2020).
- [5] O.V. Koplak, R.B. Morgunov, I.I. Khodos. *Mater. Lett.* **301**, 130291 (2021). <https://doi.org/10.1016/j.matlet.2021.130291>
- [6] O.V. Koplak, R.B. Morgunov. *Mater. Sci. Eng. B* **263**, 114845 (2021). <https://doi.org/10.1016/j.mseb.2020.114845>
- [7] E.N. Kablov, O.G. Ospennikova, D.E. Kablov, V.P. Piskorskii, R.A. Valeev, D.V. Korolev, I.I. Rezhikova, E.I. Kunitsyna, A.D. Talantsev, A.I. Dmitriev, R.B. Morgunov. *J. Exp. Theor. Phys.* **121**, 3, 429 (2015). <https://doi.org/10.1134/S1063776115090071>
- [8] E.N. Kablov, O.G. Ospennikova, V.P. Piskorskii, D.V. Korolev, E.I. Kunitsyna, A.D. Talantsev, R.B. Morgunov. *Phys. Solid State* **58**, 7, 1320 (2016). <https://doi.org/10.1134/S1063783416070180>
- [9] E.N. Kablov, O.G. Ospennikova, E.I. Kunitsyna, V.P. Piskorskii, D.V. Korolev, R.B. Morgunov. *Arch. Met. Mater.* **62**, 3, 1923 (2017). <https://doi.org/10.1515/amm-2017-0290>
- [10] E.N. Kablov, O.G. Ospennikova, V.P. Piskorskii, D.V. Korolev, E.I. Kunitsyna, A.I. Dmitriev, R.B. Morgunov. *Low Temp. Phys.* **42**, 1, 45 (2016). <https://doi.org/10.1063/1.4940226>
- [11] K. Imai, E. Masago, T. Saito, K. Shinagawa, T. Tsushima. *J. Magn. Magn. Mater.* **177–181**, 99 (1998). [https://doi.org/10.1016/S0304-8853\(97\)00936-0](https://doi.org/10.1016/S0304-8853(97)00936-0)
- [12] M. Stier, A. Neumann, A. Philipp-Kobs, H. P. Oepen, M. Thorwart. *J. Magn. Magn. Mater.* **447**, 96 (2018). <https://doi.org/10.1016/j.jmmm.2017.09.068>
- [13] Ling-Wei Li. *Chin. Phys. B* **25**, 3, 037502 (2016). <https://doi.org/10.1088/1674-1056/25/3/037502>
- [14] D. Nguyen, H. Nguyen, A. Nguyen, Y. Nguyen, T. Pham, V. Koledov, A. Kamantsev, A. Mashirov, T. Tran, H. Kieu, S. Yu. *EPJ Web Conf.* **185**, 05002 (2018). <https://doi.org/10.1051/epjconf/201818505002>
- [15] B. Dahal, P. Kharel, T. Ott, W. Zhang, S. Valloppilly, R. Skomski, D. Sellmyer. *AIP Adv.* **9**, 035211 (2019); <https://doi.org/10.1063/1.5080105>
- [16] F. Qin, H. Peng. *Rare Earths: New Research. Chapter 8. Magnetocaloric Effect of Amorphous Materials Based on Heavy Rare Earth Elements.* Nova Science, N.Y. (2020). 25 p.
- [17] P.J. von Ranke, N.A. de Oliveira, B.P. Alho, E.J.R. Plaza, V.S.R. de Sousa, L. Caron, M.S. Reis. *J. Phys. Condens. Matter* **21**, 056004 (2009). <https://doi.org/10.1088/0953-8984/21/5/056004>
- [18] L. Li. *Chin. Phys. B* **25**, 037502 (2016). <https://doi.org/10.1088/1674-1056/25/3/037502>
- [19] R. Nirmala, A.V. Morozkin, S.K. Malik. *Pramana J. Phys.* **84**, 6, 977 (2015). <https://doi.org/10.1007/s12043-015-1000-1>
- [20] D.L. Rocco, J.S. Amaral, J.V. Leitão, V.S. Amaral, M.S. Reis, S. Das, R.P. Fernandes, J.P. Araújo, A.M. Pereira, P.B. Tavares, N.V. Martins, A.A. Coelho. *J. Phys. D.* **42**, 055002 (2009). <https://doi.org/10.1088/0022-3727/42/5/055002>
- [21] K.A. Gschneidner, V.K. Pecharsky, A.O. Tsokol. *Rep. Prog. Phys.* **68**, 1479 (2005). <https://doi.org/10.1088/0034-4885/68/6/R04>
- [22] Aparna Sankar, J. AroutChelvane, A.V. Morozkin, A.K. Nigam, S. Quezado, S.K. Malik, R. Nirmala. *AIP Adv.* **8**, 056208 (2018). <https://doi.org/10.1063/1.5007696>
- [23] K. Mandal, A. Yan, P. Kersch, A. Handstein, O. Gutfleisch, K-H. Müller. *J. Phys. D.* **37**, 2628 (2004). <https://doi.org/10.1088/0022-3727/37/19/002>
- [24] K. Zehani, R. Guetari, N. Mliki, L. Bessais. *J. Phys. Procedia* **75**, 1435 (2015). <https://doi.org/10.1016/j.phpro.2015.12.163>
- [25] P.L. Dong, L. Ma, J.C. Xiong, T.Y. Chen, S.F. Lu, L. Li. *Mater. Res. Express* **6**, 126102 (2019). <https://doi.org/10.1088/2053-1591/AB455C>